Projected Complex Absorbing Potential Multi-reference Configuration Interaction Approach for Shape and Feshbach Resonances

Mushir Thodika* and Spiridoula Matsika*

Department of Chemistry, Temple University, Philadelphia, PA 19122, USA

E-mail: mushir@temple.edu; smatsika@temple.edu

Abstract

Anion resonances are formed as metastable intermediates in low-energy electron-induced reactions. Due to the finite lifetimes of resonances, applying standard Hermitian formalism for their characterization presents a vexing problem for computational chemists. Numerous modifications to conventional quantum chemical methods have enabled satisfactory characterization of resonances, but specific issues remain, especially in describing two-particle one hole (2p-1h) resonances. An accurate description of these resonances and their coupling with single-particle resonances requires a multi-reference approach. We propose a projected complex absorbing potential (CAP) implementation within the multi-reference configuration interaction (MRCI) framework to characterize single-particle and 2p-1h resonances. As a first application, we use the projected-CAP-MRCI approach to characterize and benchmark the $^2\Pi_g$ shape resonance in N_2^-. We test its performance as a function of the size of the subspace and other parameters, and we compute the complex potential energy surface of the $^2\Pi_g$ shape resonance to show that a smooth curve is obtained. One key benefit of MRCI is that it can describe Feshbach resonances (most common examples of 2p-1h resonances) at the same footing as shape resonances. Therefore, it is uniquely positioned to describe mixing between the different channels.

To test these additional capabilities, we compute Feshbach resonances in H_2O^- and anions of di-cyanoethylene isomers. We find that CAP-MRCI can efficiently capture the mixing between the Feshbach and shape resonances in di-cyanoethylene isomers, which has significant consequences for their lifetimes.

Introduction

Low-energy electron induced reactions are important in astrochemistry, condensed-phase processes, radiation damage to living cells and other processes.[1–7] Efficient inter-molecular processes due to electron impact have also been demonstrated.[8–11] When an electron interacts with a target molecule and gets trapped momentarily, anion resonances are formed. The state formed after the electron entrapment has a bound-like character within the interaction region of the molecular potential but also possesses a non-vanishing oscillating tail outside the potential. Presence of a non-vanishing tail outside the potential ensures a finite probability for auto-detachment, where the excess electron can escape back to the continuum. Depending on the electronic state of the neutral target, anion resonances can be categorized into either single-particle (1p) or two-particle one-hole (2p-1h) resonances. The decay of 1p/shape resonances in a radical anion is a one-electron process with the excess electron trapped due to the formation of a centrifugal barrier in the electron-target interaction potential (see Figure 1).[12,13] The term "shape" resonance is used to signify the peculiar shape of the interaction potential due to which the excess electron is trapped. Based on the decay mechanism, 2p-1h resonances can be further classified into "core-excited shape" or "Feshbach". The former type is energetically higher than the parent excited state and decays through a one-electron process, and the interaction potential consists of a similar centrifugal barrier. The latter type is lower in energy to the parent excited state and decays to the ground state through a two electron process, and is therefore longer-lived compared to shape resonances.

Since resonances are embedded and coupled to the continuum, application of standard bound $\mathscr{L}^2$ methods to resonances is not straightforward.[13,14] Several methods have been developed over the years for the accurate treatment of anion resonances, and with the advent of powerful com-

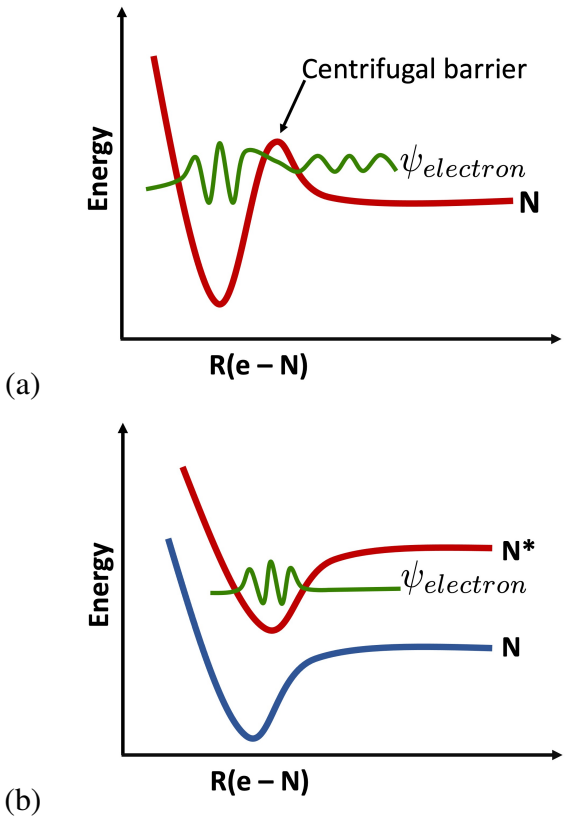

Figure 1: (a) Electron-molecule interaction potential for a shape resonance. The angular momentum barrier formed traps the excess electron. The tail of the resonance wavefunction extends beyond the barrier, thereby rendering a finite lifetime to the shape resonance. (b) The neutral ground state (blue) and the neutral excited state (red) are shown. The trapping of excess electron by the excited state of the neutral target results in the formation of Feshbach resonance.

puters and sophisticated computational algorithms, computing anion resonances of polyatomic systems with increased accuracy has gained more traction.[14–20] Explicit treatment of the continuum is possible in scattering theory and hence, methods based on scattering theory,[17,19,21–26] have established themselves as powerful tools for studying anion resonances and dissociative electron attachment phenomena. On the other hand, numerous modifications to standard Hermitian electronic structure theory have also enabled plethora of studies on resonances.[14,16,18,20,27] Electronic structure theory based methods have the advantage of being more user-friendly for a quantum chemist compared to scattering methods, and also enable chemical interpretation of the states in terms of Dyson orbitals, Frank-Condon factors and so on.[20] Within the formalism of electronic structure theory, non-Hermitian quantum mechanical methods, such as complex scaling, complex

absorbing potentials (CAP), exterior complex scaling, and complex basis functions, have been explored extensively.[13,16,20,27–34] The equivalence between all the non-Hermitian quantum mechanical based methods is illustrated neatly in the work by Ben-Asher and Moiseyev.[35] In a non-Hermitian method, the analytic continuation of the physical Hamiltonian to the complex plane makes the wavefunction of resonance states square-integrable.[13,16] It must be noted that although complex scaling and reflection-free CAPs represent analytic continuations of the Hamiltonian to the complex plane, the addition of a box-CAP doesn't. The resonance states thus obtained, are bound states of the non-Hermitian Hamiltonian with complex eigenvalues,[13]

$$E = E_R - i\frac{\Gamma}{2}. \tag{1}$$

The complex energies (or Siegert energies as they are commonly known[36]) encompass the information on the position and lifetime of the resonance state. The real part of the Siegert energy gives the resonance position, and the imaginary part corresponds to the half-width of the resonance. The inverse of the full-width (Γ) gives the lifetime of the resonance

$$\tau = \frac{\hbar}{\Gamma} \tag{2}$$

Analytic continuation can also be introduced at the eigenvalue level, as seen in orbital stabilization methods and extrapolation methods, and consequently one can completely avoid the use of non-Hermitian quantum chemistry.[18,37] Complex absorbing potentials[20,27,33,34] have found huge success compared to other non-Hermitian methods for the computation of auto-ionizing states. In the CAP formalism, the physical Hamiltonian of a system is augmented with a complex local potential, resulting in a purely discrete spectrum.[33] Resonances are then obtained as square-integrable eigenfunctions of the non-Hermitian Hamiltonian with Siegert energies.[33] The success of CAP based methods can be attributed to the ease of integration with any available electronic structure method. Methods augmented with CAP include coupled cluster (EOM-CC and FSMRCC), algebraic diagrammatic construction schemes (ADC), Symmetry Adapted Cluster/Configuration

Interaction (SAC-CI), multi-reference configuration interaction (MRCI), multi-reference perturbation theory (XMCQDPT2, XMS-CASPT2), electronic propagator (EP) and density functional theory (DFT).[38–55] Several properties such as complex Dyson orbitals and natural transition orbitals, as well as analytic gradients, and algorithms for locating crossing points have also been developed within CAP.[56–59] Recent implementation of analytic gradients within the CAP-EOM-CC formalism has enabled computation of optimized structures and exceptional points. Optimized structures and adiabatic electron affinities have been computed for several polyatomic systems such as formaldehyde, formic acid and ethylene anions using the CAP-EOM-CC formalism.[56] Recently, CAP-EOM-CC has also been employed to compute minimum energy exceptional points on crossings between resonances and minimum energy crossing points between neutral and anionic surfaces.[57,58] The routine application of a variety of CAP augmented methods to compute resonances serves as a testament to their success compared to other non-Hermitian or even Hermitian methods.

The conventional implementation involves adding CAP at the Hartree-Fock stage and working through the complex algebra for the inclusion of electron correlation. To accommodate the complex algebra as a consequence of the non-Hermiticity of the CAP augmented Hamiltonian, the familiar concepts of normalization, orthogonalization have to be redefined.[13] An obvious consequence of having to deal with complex numbers within the electronic structure framework is the increase in associated computational cost and memory requirements.[13] In addition, the resonance eigenvalues are also dependent on a set of user-defined CAP parameters, and as a result, multiple electronic structure calculations are required for the optimization of parameters to obtain optimum results. The combination of these factors with very diffuse basis sets (a general requirement for anions) greatly enhances the computational cost in conventional implementation of CAP, making it expensive for the computation of resonances in large polyatomic systems.[60] An easier way to circumvent the high cost and memory requirements associated with conventional CAP is to project the CAP to a subspace spanned by the eigenstates of the physical Hamiltonian at the correlated level.[61] The resulting small complex symmetric matrix can be easily diagonalized with standard

diagonalization routines. This approach has the definite advantage of being very efficient in terms of computational cost compared to the traditional CAP procedure, as only one electronic structure calculation (albeit of many states) is needed to generate the underlying subspace. Studies have shown that projection schemes are very much capable of reproducing results obtained from conventional schemes and in many cases can generate smooth potential energy surfaces associated with resonances.[44,47,50,51] When using the projection scheme it is important to check the convergence of the results against the size of the effective Hamiltonian. A recent study by Dempwolff et al. on characterization of anion resonances with CAP-ADC using the projection scheme has shown that one can reproduce accurate resonance energies and widths of conventional CAP approach with a small subspace.[44] While projected CAP offers numerous advantages, certain drawbacks do exist. For example, it is not clear that complex potential energy surfaces and their gradients will always be smooth for polyatomic molecules compared to conventional CAP. It is also possible that in certain cases (higher-lying resonances), the computed resonance parameters display significant variation with the effective Hamiltonian size.[55]

Most studies on application of CAP for computing anion resonances in polyatomic systems have often focused on the computation of low-lying shape resonances. The computation of high-lying shape and Feshbach resonances is important as they are known to facilitate a variety of electron-driven reactions.[62–70] Furthermore, the prevalence of the resonant-channel coupling in nucleobases and other aromatic systems warrants more investigation as such phenomena perhaps could be the key to unravelling the fundamental pathways in radiation damage of bio-molecular systems.[69–73] Resonant-channel coupling is usually observed between a shape and a Feshbach resonance of the same symmetry in an anion. Estimation of this coupling requires obtaining both shape and Feshbach resonances in the same calculation, and this is where multi-reference methods are essential. One strong advantage of multi-reference methods is that both shape and Feshbach resonances and the coupling between them can be obtained in the same calculation.[71,72,74,75,75,76] In addition, one can also generate the complete potential energy surfaces (PES) for resonances with

CAP augmented multi-reference methods, unlike single reference methods where one can only generate the PES in the vicinity of the equilibrium structure of the resonance.[51] There have been some recent implementations of CAP with multi-reference methods, focusing mostly on multi-configurational perturbation theory or MCSCF.[50–52,59] An earlier implementation combined CAP with MRCI and examined the applicability of the projection scheme.[48,61] That work however did not integrate CAP with a generally available MRCI code restricting its applicability. Our goal in this work is to generate and test a CAP-MRCI approach using an easily available electronic structure code with analytic gradients available, with a future goal of applying it to polyatomic molecules and electron driven chemistry. In this work, we implement and benchmark a projected CAP-MRCI method to study primarily 2p-1h resonances and resonant channel coupling. The uncontracted version of the MRCI as implemented in the COLUMBUS[77,78] system is used for the electronic structure calculations. Unlike the previous implementation,[48] the current implementation of CAP-MRCI uses the open-source COLUMBUS electronic structure program system as the underlying package, which is interfaced to the freely available openCAP program.[79] The combination of openCAP and COLUMBUS programs provides a user-friendly experience for the computation of anion resonances with multi-reference approaches. At first, the new projected CAP-MRCI method is used to characterize the well-studied $^2\Pi_g$ shape resonance of N_2 anion. by computing the PES of the $^2\Pi_g$ resonance in N_2^-. A systematic study on the dependence of N_2^- resonance parameters on subspace size, basis set, and Davidson convergence tolerance is shown. Following the benchmark of N_2^-, we study the $^2B_1$ Feshbach resonance in H_2O^-. For the $^2B_1$ resonance in water anion, we also examine the dependence of resonance parameters on the chosen active space. Finally, we use the projected CAP-MRCI approach to compute both Feshbach and shape resonances in cis- and trans- isomers of dicyanoethylene, where we have the opportunity to investigate the resonant-channel coupling between the shape and Feshbach resonances in both isomers.

Methods

Background theory

Complex Absorbing Potential

The use of complex absorbing potentials to compute atomic and molecular resonances is built on a rigorous mathematical foundation provided by Riss and Meyer.[33] A complex local potential is added to the physical Hamiltonian H as shown in Eqn 3.[33]

$$H(\eta) = H - i\eta W \tag{3}$$

W is the one-particle CAP and η is the potential strength. Traditionally, CAP augmented calculations have often employed a "box-like" potential, where the potential is zero inside the box and grows quadratically outside the box.[42,49,61,80,81] Box-CAP is employed routinely due to the simplicity involved in the evaluation of one-electron integrals. Aside from box-CAP, elliptical-CAPs and smooth Voronoi CAPs are also available.[33,82,83] In particular, smooth Voronoi CAP is generally better than box-CAP as it has the same symmetry as that of the physical Hamiltonian, it conforms to the shape of the molecule, and is therefore better suited for describing resonances in polyatomic systems and molecular clusters.[81,83,84] Nevertheless, the use of Voronoi CAP is limited owing to difficulties arising from numerical evaluation of the one-electron integrals. In our work, we have employed the "box" potential for all our calculations:[80]

$$W = \sum_{i=x,y,z} W_i \tag{4}$$

where,

$$W_i = \begin{cases} 0 & \forall \ |r_i| < r_i^0 \\ (|r_i| - r_i^0)^2 & \forall \ |r_i| > r_i^0 \end{cases} \tag{5}$$

The form of the potential is such that it is zero inside the interaction region of the molecular potential and has a finite value outside the interaction region. The separation between the off and on regions is decided by the user specified cut-off parameter 'r_i^0' in Eqn 5. This separation ensures that the bound states are not perturbed much by the introduction of the artificial potential. The Siegert energies associated with resonance states are obtained directly as eigenvalues of the non-Hermitian Hamiltonian. In the complete basis set limit, the true Siegert energy of a resonance state is obtained in the limit of $\eta \rightarrow 0_+$. However, the inevitable use of finite basis sets means that a finite value of CAP strength is required to stabilize the resonances.

As the CAP strength is increased, the eigenvalues of the CAP augmented Hamiltonian move into the complex plane. In particular, the eigenvalues of the resonance state computed as a function of CAP strength tend to accumulate in a certain region of the complex plane. The optimal CAP strength is then identified as the point at which the logarithmic velocity is at its minimum. In other words, the stabilized point at which the optimal CAP strength is obtained corresponds to minimization of the first order term in the Taylor series expansion of the η dependent energy:[27]

$$|E(\eta) - E(0)| = \left| \eta \frac{dE}{d\eta} \right| + \mathscr{O}(\eta^2) \tag{6}$$

Graphically, the point at which the first-order term is at its minimum corresponds to a turning point in the η-trajectory of the resonance. To further reduce the sensitivity of computed Siegert energies to changes in the CAP onset, few strategies have been reported in the literature. The underlying idea is to improve the energy by minimizing higher order terms in the Taylor series expansion of η-dependent energy. In this work, we have employed the correction scheme introduced by Riss and Meyer where we subtract the energy derivatives from the zeroth order energy. Another correction scheme introduced by Krylov and co-workers accomplishes the same but with the use of density matrices, where the energy-derivatives are re-computed in terms of expectation value of the CAP operator by the use of Hellman-Feynman theorem.[85] Both correction schemes tend to provide similar results but it is seen that the density based correction scheme could be useful in

certain cases.[55] Based on the scheme introduced by Riss and Meyer,[33] the first order corrected energy 'U' is defined as

$$U = E(\eta) - E(0) - \eta \frac{dE(\eta)}{d\eta} \tag{7}$$

The minimization of the second-order term identifies the turning point in the η-trajectory for corrected energies (U):[20]

$$min \left| \eta^2 \frac{d^2E}{d\eta^2} \right| = min \left| \eta \frac{dU}{d\eta} \right| \tag{8}$$

In this work, the optimum energy obtained from the minimization of the first-order term will be henceforth referred to as the uncorrected energy (E) and as per Eqn 7, the second-order minimized energy will be referred to as the corrected energy (U).

Implementation of projected CAP-MRCI

In this work, we employ the projected CAP approach for implementation at the MRCI level. First we solve the $(N+1)$-electron Hamiltonian at the MRCI level for a set of eigenpairs $\{(\Psi_\nu, E_\nu), \nu = 1, \ldots\ldots, K\}$,

$$H\Psi_\nu = E_\nu \Psi_\nu \tag{9}$$

Following this, the CAP matrix is represented in a Gaussian basis set,[61]

$$\langle \chi_a | W | \chi_b \rangle = \int \chi_a(\mathbf{r}) W(\mathbf{r}; \mathbf{r}^0) \chi_b(\mathbf{r}) d\mathbf{r} \tag{10}$$

where χ is a Gaussian-type function, and W is the complex absorbing potential as given in Eqn 5. The computed CAP matrix in atomic orbital (AO) basis is then transformed into the molecular orbital (MO) basis using the converged MO coefficients obtained from the underlying self-consistent field calculation of the $(N+1)$-electron system. In our case, we employ the converged orbitals from a CASSCF calculation. The molecular orbitals are represented in terms of Gaussian atomic orbitals as $\phi_p = \sum_a C_{ap} \chi_a$. Following this, the CAP integrals can now be represented in the MO

basis,[27,61]

$$\langle \phi_p | W | \phi_q \rangle = \sum_{a,b} C_{ap} \langle \chi_a | W | \chi_b \rangle C_{bq} \tag{11}$$

where 'p' and 'q' indices run over MOs and 'a' and 'b' indices run over AOs. Once the CAP matrix is represented in the MO basis, the CAP augmented Hamiltonian (see Eqn 3) is projected onto the subspace spanned by the set $\{\Psi_{p_1}, \Psi_{p_2}, \ldots\ldots, \Psi_{p_K}\}$,[27,61]

$$\Psi^{\dagger}_{p_\lambda} H(\eta) \Psi_{q_\nu} = E_{p_\lambda} \delta_{\lambda\nu} - i\eta \Psi^{\dagger}_{p_\lambda} W \Psi_{q_\nu} \tag{12}$$

where '$\lambda, \nu = 1, ..., K$', with 'K' being the total number of computed roots at the MRCI level of theory. Once the final Hamiltonian is projected onto the subspace spanned by the eigenvectors of K roots, the resulting small complex symmetric matrix is diagonalized for a series of CAP strengths to obtain the desired η-trajectories. The electronic structure energies and wavefunctions are obtained from the COLUMBUS program system,[77,78,86,87] and the resonance trajectories are generated and analyzed with the help of the OpenCAP package.[79]

Electronic structure methods

Most electronic structure calculations in this work are performed at the MRCI level with single excitations (MRCIS), while we tested the performance of single and double excitations (MRCISD) in the case of the N_2^- resonance. There are no frozen orbitals at the MRCI level. As demonstrated earlier in a previous work,[51] initially a calculation for the neutral ground state of the molecule is performed at the state-averaged CASSCF (SA-CASSCF) level with a valence active space to generate the optimized orbitals for subsequent calculations. In the next step, the valence active orbitals are augmented with a set of lowest energy diffuse orbitals (n_{virt}) to perform a SA-CASSCF and MRCIS calculation on the anion.

Obtaining a balanced approach between the neutral and anion energies is challenging with multi-reference methods. There is no unique way to do this, but using the same set of orbitals for both neutral and anion has been used before with improved results, and that is the approach

we chose here.[51] The converged orbitals of the anion are used to perform MRCI on the neutral to obtain the reference energy in order to calculate electron attachment energies. In another approach, one can add a very diffuse function (exponent $\approx 10^{-5}$-10^{-8}) on one of the atoms and obtain the position in a single calculation where the lowest state in the anion calculation corresponds to neutral plus the excess electron occupying a very diffuse orbital.[50]

N_2 methodology

For N_2, the N-N bond distance is optimized to be 2.078 bohr at the B3LYP/aug-cc-pVTZ level of theory. For the CASSCF on the neutral N_2, a (4,4) active space is employed with state-averaging over 8 states. The active space used in the CASSCF calculation for the neutral consists of the degenerate pairs of π and π^* orbitals. In the anion calculations, the (4,4) active space is augmented with two degenerate pairs of diffuse orbitals of π symmetry, leading to a (5,8) CAS, and an average over 10 states is used (SA10-CASSCF). The active space orbitals can be found in Fig S1 of the supplementary information (SI). The parent basis set, Dunning's correlation-consistent triple-zeta basis, aug-cc-pVTZ is placed on both the nitrogens. The diffuse functions are either added on a ghost atom in the center of the molecule or on the nitrogen atoms. A set of [3s3p3d] and [5s5p5d] functions are placed on the ghost atom to generate two ghost-atom based basis sets: aug-cc-pVTZ+gh[3s3p3d] and aug-cc-pVTZ+gh[5s5p5d]. For the atom-centered type, the parent basis aug-cc-pVTZ is augmented with the addition of either [3s3p] or [2s2p2d] functions. The diffuse functions in all basis sets are obtained in an even-tempered manner ($\alpha_{i+1} = 0.5\alpha_i$), where '$\alpha_i$' is the exponent of the most diffuse function for a given angular momentum in the parent basis set.

H_2O methodology

The equilibrium structure of the neutral water molecule was obtained at the MP2/aug-cc-pVTZ level of theory. The electronic configuration of neutral water is $1a_1^2 2a_1^2 1b_2^2 3a_1^2 1b_1^2 4a_1^0 2b_2^0$, based on the C_{2v} abelian point group. The aug-cc-pVTZ basis set is added on all the atoms and an

additional even-tempered set of [3s3p3d] Gaussians is placed on the oxygen atom. Prior to the anion calculation, a CASSCF calculation on the neutral H_2O molecule is performed with a (6,5) active space and state-averaging over 10 states. The base active space of (6,5) consists of the orbitals $3a_1$, $4a_1$, $1b_2$, $1b_1$ and $2b_2$ orbitals. For the anion calculations, the active set employed in the neutral water CASSCF is augmented with 2, 3 or 4 lowest energy virtual orbitals of b_1 symmetry to create three different active spaces, and a SA10-CASSCF is used.

Dicyanoethylene methodology

The structures of maleonitrile (cis-dicyanoethylene) and fumaronitrile (trans-dicyanoethylene) are optimized using B3LYP/cc-pVTZ. A (6,6) active space consisting of all the valence out-of-plane π and π^* orbitals is used in the CASSCF calculations on the neutral for both isomers. The state-averaging for both the neutral calculations is performed over the first 10 states. The valence active orbitals used for the CASSCF calculations on both isomers are summarized in Figs S2 and S3 of the SI. Once again, Dunning's correlation consistent triple-valence zeta basis set with augmentations (aug-cc-pVTZ) is used as the parent basis set on all the atoms. A set of even-tempered [3p] functions is added on the carbon (C) and nitrogen (N) atoms of both isomers. The active space used in the CASSCF and subsequent MRCIS calculations on the anion and the neutral reference is augmented with 3 diffuse functions of the same symmetry as that of the resonance. This leads to an active space of (7,9) for the anion and (6,9) for the neutral. For the anion CASSCF and MRCIS calculations, the state-averaging is performed over the first 12 states.

Results and Discussion

$^2\Pi_g$ shape resonance in N_2 anion

First, we look at the well studied $^2\Pi_g$ shape resonance in the N_2 anion. An accurate fixed-nuclei estimate based on the experimental data reports the $^2\Pi_g$ resonance position at 2.32 eV and the width at 0.41 eV.[88] Being one of the model systems for studying new methods developed for

anion resonances, numerous theoretical predictions of the resonance parameters for the $^2\Pi_g$ shape resonance with a variety of methods have been reported in the literature. Table 1 summarizes some of the previous predictions of the resonance parameters for the lowest N_2 anion shape resonance. From Table 1, the reported positions and widths vary between 2.23-3.12 eV and 0.25-0.65 eV, respectively.

Table 1: Selected previous theoretical predictions of the $^2\Pi_g$ resonance in N_2 anion.

Method	E_R/eV	Γ/eV
Stieltjes-moment theory-CIS[89]	2.23	0.40
Optical potential-ADC(3)[90]	2.53	0.54
CAP-MRCISD[49]	2.97	0.65
CAP-FSMRCC[43]	2.52	0.39
CAP-EOM-EA-CCSD[42]	2.57	0.25
OSM-EOM-EA-CCSD[60]	2.52	0.49
CAP-EP-MCSCF[52]	3.12	0.31

Our values for the $^2\Pi_g$ resonance in N_2^- are tabulated in Table 2 for several box sizes. The corresponding trajectories for the box size $r_x^0 = r_y^0 = 2.76, r_z^0 = 4.88$ bohr are shown in Figure 2. The change in corrected positions and widths with box size is less significant than that of the uncorrected results, as expected. Nonetheless, the resonance parameters remain more or less consistent with small variations at both the uncorrected and corrected level.

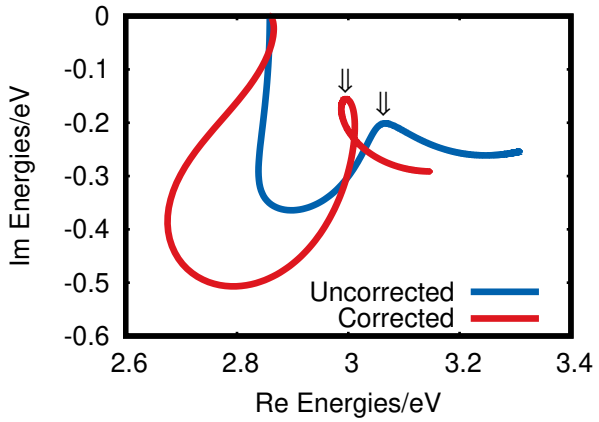

Figure 2: Uncorrected and corrected trajectories of the $^2\Pi_g$ resonance in N_2 anion at CAP-MRCIS(5,8)/aug-cc-pVTZ+gh[3s3p3d] level of theory. The minima of first and second order logarithmic velocities corresponding to uncorrected and corrected trajectories, respectively, are indicated by the arrows. The box size used is $r_x^0 = r_y^0 = 2.76, r_z^0 = 4.88$ a.u.

Table 2: Uncorrected and corrected energies, widths and optimum η for the $^2\Pi_g$ resonance in N_2 anion using CAP-MRCIS(5,8)/aug-cc-pVTZ+gh[3s3p3d] for various box sizes.

Box size (a.u.)	E_R(eV)	Γ (eV)	η^E_{opt} (a.u.)	U_R (eV)	Γ(eV)	η^U_{opt} (a.u.)
$r^0_x = r^0_y = 2.76, r^0_z = 4.88$	3.06	0.40	0.0095	3.00	0.31	0.018
$r^0_x = r^0_y = 3.00, r^0_z = 5.00$	3.05	0.38	0.011	2.99	0.29	0.021
$r^0_x = r^0_y = 4.00, r^0_z = 5.00$	3.02	0.31	0.021	2.97	0.23	0.041

Our positions agree well with the CAP-MRCISD and CAP-EP-MCSCF results of Sommerfeld et al.[51] and Das et al.,[52] as listed in Table 1. In multi-reference methods, the position is generally computed by taking the difference between the energies of the anion and the neutral. The difference in correlation between anionic and neutral calculations leads to uncertainties in the final result, and that probably explains why both our results and the previous MCSCF results somewhat overestimate the position compared to experiment.

The width of $^2\Pi_g$ resonance shows great variation among the previously reported values. When compared to the fixed-nuclei estimate of 0.41 eV by Berman et al.,[88] our theoretical prediction is somewhat underestimated depending on the box size. Obtaining widths experimentally can be complicated due to its sensitivity to nuclear positions. In certain cases, the sensitivity of widths to nuclear position can be rather severe, which makes the comparison between theoretical and experimental estimates difficult. The reported positions and widths vary between 2.23-3.12 eV and 0.2-0.4 eV respectively. Compared to previous estimates, they fall well within the range of theoretical values reported in the literature.

Tolerance dependence

Since the projected CAP approach is dependent on the size of the subspace, it is also crucial to assess the effect of convergence of pseudo-continuum states on the computed resonance parameters. In COLUMBUS, the CI matrix diagonalization is carried out using the iterative Davidson-Liu diagonalization algorithm.[91,92] The energy convergence for different excited states is decided by setting the residual tolerance vector for each state. A residual norm of 10^{-n_r}, where $n_r \geq 3$ results in stronger convergence of the computed roots. In this study, we have employed four sets of tolerance

conditions as tabulated in Table 3, where the individual residual vector norms are adjusted in every set. A tolerance level of $1e-3$ implies stronger convergence and levels of $1e-2$ or $1e-1$ imply loose convergence. In all the tolerance sets, the resonance state has a minimum energy convergence of 10^{-11} Hartree. The distinction between the resonance and the pseudo-continuum state comes by looking at the coefficients of the CI vector corresponding to a given electronic configuration in a CAP free calculation. When a state is identified as the resonance state, it means that particular state has dominant contributions from the CI vector corresponding to the electronic configuration of the resonance. In some cases the contribution may not be as clear however complicating this analysis.

Table 3: Tolerance sets employed for the computation of the $^2\Pi_g$ resonance energy and width in N_2^- at SA10-CASSCF/SA10-MRCIS(5,8)/aug-cc-pVTZ+gh[3s3p3d] level of theory. The tolerance 'n_r' for the individual roots 1 through 10 is shown. Root 2 has the electronic configuration of the resonance state, while the other roots are pseudo-continuum states. Tolerance for the resonance is set to high value while the tolerance of the other roots is explored.

Tol. index	1	**2**	3	4	5	6	7	8	9	10	Niter
1	1e-3	**1e-3**	1e-3	1e-3	1e-3	1e-3	1e-3	1e-3	1e-3	1e-3	253
2	1e-3	**1e-3**	1e-3	1e-3	1e-3	1e-2	1e-2	1e-2	1e-2	1e-2	154
3	1e-2	**1e-3**	1e-2	1e-2	1e-2	1e-2	1e-2	1e-2	1e-2	1e-2	205
4	1e-1	**1e-3**	1e-1	1e-1	1e-1	1e-1	1e-1	1e-1	1e-1	1e-1	36

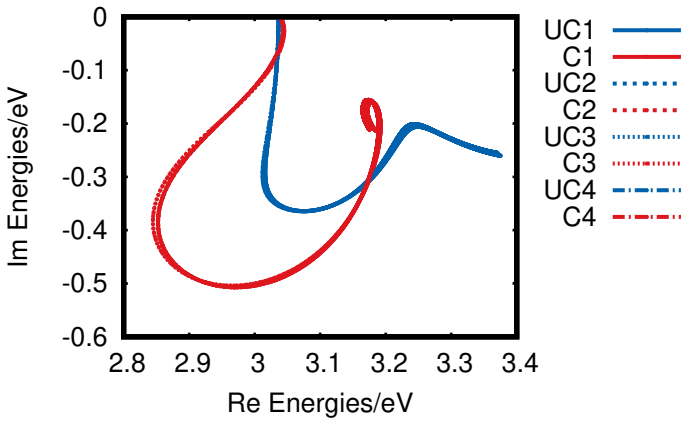

Figure 3: Uncorrected (UC) and corrected (C) trajectories for the $^2\Pi_g$ resonance in N_2 anion at MRCIS(5,8)/aug-cc-pVTZ+gh[3s3p3d] level of theory for difference tolerance sets, denoted as UCi and Ci where i is the tolerance index in Table 3.

Table 4: Uncorrected and corrected energies, widths and optimum η of the $^2\Pi_g$ resonance in N_2 anion at CAP-MRCIS(5,8)/aug-cc-pVTZ+gh[3s3p3d] level of theory for various tolerance sets. Box size is set at $r_x^0 = r_y^0 = 2.76, r_z^0 = 4.88 a.u.$.

Tol. index	E_R (ev)	Γ (eV)	η^E_{opt} (a.u.)	U_R (eV)	Γ(eV)	η^U_{opt} (a.u.)
1	3.06	0.40	0.0095	3.00	0.31	0.018
2	3.06	0.40	0.0095	3.00	0.31	0.018
3	3.06	0.40	0.0095	3.00	0.31	0.018
4	3.07	0.41	0.0095	3.00	0.32	0.018

Figure 3 summarizes the trajectories obtained at various tolerance sets. It is clearly seen that all the trajectories are seemingly on top of each other with minimal variation. The reported values for energy position and width as summarized in Table 4 indicate that there is barely any change in the reported values when the pseudo-continuum states are not as accurately converged compared to the resonance state. A small change of 0.01 eV in the position and width is seen at the lowest tolerance setting which is once again quite minimal. It is worth noting that the energy position and width reported at the lowest tolerance setting is obtained in a mere 36 iterations of the Davidson-Liu algorithm compared to 253 for the highest tolerance setting. This further cements the fact that in CAP, only the resonance state needs to be accurately represented unlike the stabilization method, where the final position is strongly dependent on the energy convergence of the pseudo-continuum states. Also, by smartly adjusting the convergence threshold of pseudo-continuum states, one can easily perform the calculation for a higher subspace size and have it converge faster. Adjusting the tolerance thresholds can also be helpful in computing resonances in fairly larger systems, where the iterations are usually slower and the pseudo-continuum states are difficult to converge as well.

Effect of subspace size, basis sets, and correlation

To check the dependence of the resonance parameters as a function of the subspace size, we report the positions and widths of the $^2\Pi_g$ shape resonance for increasing number of states at the MRCIS level of theory. Figure 4 summarizes the change in the computed positions and widths respectively as a function of the number of states included in the CAP Hamiltonian. It is worth noting that the resonance position remains constant for up to 30 states in the subspace size. The widths also

remain more or less consistent, although there is somewhat more sensitivity.

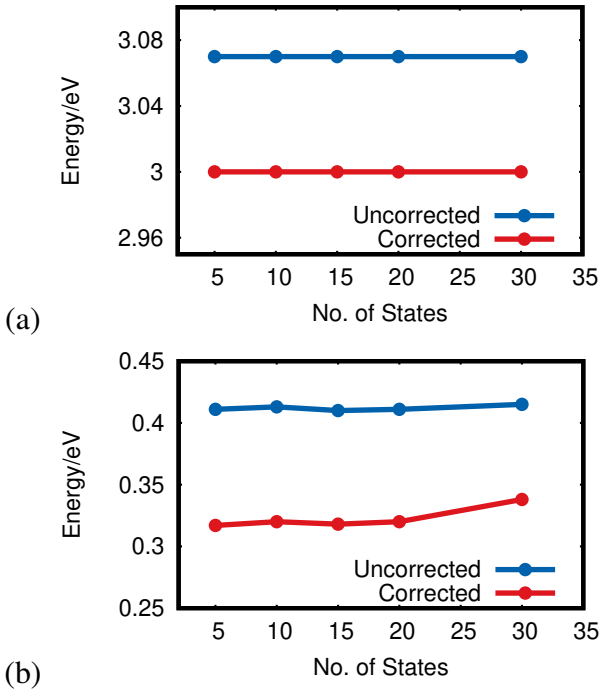

Figure 4: (a) Resonance positions and (b) resonance widths of $^2\Pi_g$ resonance in N_2^- as a function of subspace size at MRCIS(5,8)/aug-cc-pVTZ+gh[3s3p3d] level of theory.

To check the effects of basis sets on resonance parameters, we benchmarked the complex energies for four basis sets. We used Dunning's augmented correlation-consistent valence triple-zeta (aug-cc-pVTZ) as the parent basis set. The four sets of basis set employed included a pair of atom-centered and a pair of ghost-atom based basis sets, respectively. The results are summarized in Table 5. Based on these results there seems to be an overall uncertainty of 0.1 eV in both positions and widths because of the basis set. The basis set dependence for various CAP implementations has been explored previously in the literature,[42,50] so we are not focusing any further on this issue.

Finally, we explored the effects of correlation by introducing the double excitations at the MRCI level. The differences between the final resonance positions and widths obtained for the $^2\Pi_g$ resonance is summarized in the supporting information using SA5-MRCI(5,8)/aug-cc-pVTZ+gh[3s3p3d]. The widths at the MRCISD level decrease by 0.1 eV in comparison to the MRCIS widths both at the uncorrected and the corrected level and show more agreement with the CAP-EOM-CC results

Table 5: Uncorrected and corrected energies, widths, and optimum η of the $^2\Pi_g$ resonance in N_2 anion at CAP-MRCIS(5,8) level of theory. Results are shown for both atom-centered and ghost-atom based basis sets. All results are shown for a box size of $r_x^0 = r_y^0 = 2.76, r_z^0 = 4.88 a.u.$

Basis Set	E_R (ev)	Γ (eV)	η_{opt}^E (a.u.)	U_R (eV)	Γ(eV)	η_{opt}^U (a.u.)
aug-cc-pVTZ+[3s3p]	3.08	0.32	0.0067	3.03	0.20	0.014
aug-cc-pVTZ+[2s2p2d]	3.03	0.46	0.0039	2.95	0.44	0.0071
aug-cc-pVTZ+gh[3s3p3d]	3.06	0.40	0.0095	3.00	0.31	0.018
aug-cc-pVTZ+gh[5s5p5d]	3.12	0.33	0.010	3.07	0.24	0.020

of Zuev et al.[42] The decrease in widths associated with increase in correlation is counter-intuitive but has been observed before as well. Jagau et al.[93] found that the inclusion of triple excitations at the EOM-CC level decreased the widths compared to the values obtained at the EOM-CCSD level for all resonances studied. The resonance position obtained at the MRCISD level is over-estimated in comparison with the position at the MRCIS level by 0.4 eV. As a result, the position at the MRCISD level is significantly over-estimated in contrast to previously reported theoretical and experimental positions. The most likely reason for this increased uncertainty of the resonance position is the addition of significant correlation energy to both neutral and anionic species due to the inclusion of both single and double excitations at the MRCI level which exaggerates the problem of differential correlation. The differential correlation error is relatively lower when only single excitations at the MRCI level are included, and, as a result, we have mainly focused on MRCIS for characterizing resonances in this work.

Continuum remover CAP

The use of continuum remover CAP (or CR-CAP) to weed out non-physical stabilization points in CAP trajectories was first proposed by Sajeev *et al.*.[94] In CR-CAP, a real potential is also added to the Hamiltonian in addition to the complex potential. The final Hamiltonian is given as:[94]

$$H = H + (\lambda - i\eta)W \tag{13}$$

where 'λ' is the strength of the real potential. The real potential is also "turned on" in the same region as that of the CAP. The appearance of the non-physical stabilization is attributed to the incomplete damping of the wavefunctions in the absorbing region. Since the wavefunctions associated with continuum states have high amplitudes in the absorbing region compared to resonance states, the real potential perturbs the continuum states to a greater extent while the resonance state remains unaffected.

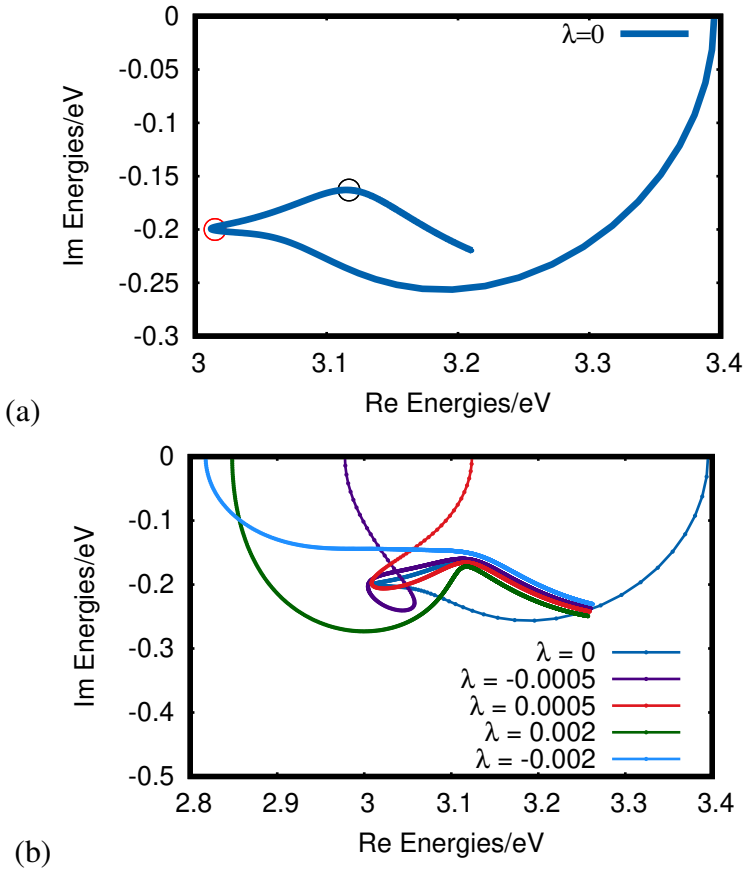

Figure 5: (a) Uncorrected trajectory for the $^2\Pi_g$ resonance in N_2 anion for $\lambda = 0$ using MRCIS(5,8)/aug-cc-pVTZ+gh[5s5p5d] level of theory. At $\lambda = 0$ two stabilization points (or turning points) are observed. The turning points are marked with red and blue circles. (b) Uncorrected trajectories for a finite value of the real potential.

We demonstrate the utility of CR-CAP in the uncorrected trajectory for the $^2\Pi_g$ resonance in N_2^- computed at MRCIS(5,8)/aug-cc-pVTZ+gh[5s5p5d] level of theory which has two stabilization points, as seen in Figure 5a. To identify the physical stabilization point on the trajectory, a finite value is assigned to the λ parameter. As seen in Figure 5b, the non-physical stabilized point

starts to disappear as λ is increased. Moreover, there is significant difference in the shape of the trajectories in the region where $\eta \leq \eta_{opt}$. Once the trajectories corresponding to different strengths of the real potential cross the actual physical stabilization point corresponding to η_{opt}, they all follow the same pattern. By employing the CR-CAP approach, we were able to determine the real turning point and therefore, the stabilized resonance parameters. It should be noted that there is no need to optimize the strength of the real potential. We usually pick small values (positive or negative) and increase them until the non-physical stabilization points start to disappear. Beyond a certain arbitrary limit, the strength of the real potential can result in un-physical perturbations of the trajectories.

Complex potential energy surface of the $^2\Pi_g$ resonance in N_2^-

To ensure that the CAP-MRCI approach can be used beyond just the single point characterization of resonances, it is important that the method is capable of producing smooth complex potential energy surfaces of the metastable anions. Computing PES of metastable anions with CAP methods is precarious as the final result depends on parameters such as CAP strength and onset. The optimum parameters are dependent on the geometry of the molecule and therefore kinks and inconsistencies in the potential energy surfaces are expected. Previous studies with CAP augmented methods have shown to yield smooth and consistent potential energy surfaces,[51,95] but that is not always the case, as seen in the case of CPES of $^2\Sigma_u^+$ resonance of H_2 [95] and minimum energy crossing pathway of π^* resonance of formic acid with the corresponding ground state of neutral.[57] It has recently been observed that in certain cases, even the choice of correction scheme for the determination of η_{opt} can play a role in affecting the integrity of the PES.[55] Furthermore, the projected CAP introduces additional variations, such as the size of subspace.

Here, to demonstrate the application of CAP-MRCI as a useful tool for the exploration of complex potential energy surfaces, we investigate the PES of the well studied $^2\Pi_g$ shape resonance in N_2^-. The CAP onset is determined based on the $\langle R^2 \rangle$ values for the equilibrium structure of ground state N_2 and is fixed at $r_x^0 = r_y^0 = 2.76\ a.u.$, $r_z^0 = 4.88 a.u.$, respectively. For a Π type

resonance, it is safe to assume that the resonance parameters are not oversensitive to change in the CAP onset. However, when dealing with a σ type resonance, the CAP onset should be optimized along with the CAP strength at each point.[95]

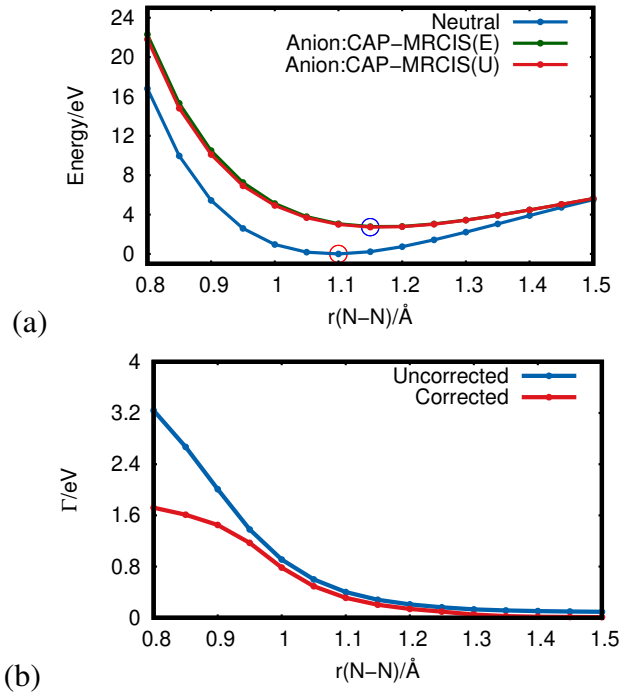

Figure 6: (a) Potential energy curves of the $^1\Sigma_g^+$ state of N_2 and the $^2\Pi_g$ state of N_2^- at MRCIS(5,8)/aug-cc-pVTZ+gh[3s3p3d] level of theory. The encircled red and blue points correspond to the equilibrium bond distance (r_{eq}) on neutral and anionic surfaces, respectively. (b) Corresponding widths along the PES

From our CAP-MRCIS calculations, a smooth potential energy surface is obtained for the $^2\Pi_g$ state as summarized in Figure 6. A shallow minimum is seen on the anionic PES at r(N-N) = 1.15 Å. As expected, the optimum geometry of the anion is slightly displaced along the reaction coordinate compared to the optimized neutral structure. The complex PES obtained at the CAP-MRCIS level is in fairly good agreement with the PES obtained by Jagau et al.[95] and White et al.[32] at EOM-EA-CCSD level of theory. A small difference is however observed near the crossing point between our results and the EOM-EA-CCSD results.[32,95] The crossing between the neutral and the anion curves in this work is observed close to $\approx$ 1.55 Å whereas the crossing point is seen at $\approx$ 1.45 Å at the coupled cluster level. The width of the resonance as a function of bond length is

shown in Figure 6b. A difference between the uncorrected and corrected widths starts to increase at shorter bond lengths. The uncorrected width increases in a strictly linear fashion to 3.2 eV at 0.8 Å whereas the corrected width undergoes a gradual increase and attains a width of $\approx$ 1.6 eV at 0.8 Å. More importantly, the corrected width becomes zero at the same distance as the crossing between the neutral and the anion surfaces, as is physically expected.

The PES obtained for the $^2\Pi_g$ resonance at the projected CAP-MRCI level agrees well with previous studies with respect to the shape and the continuity of the PES, thereby demonstrating the capabilities of the projected approach to computing complex PES. One strong advantage of using MRCI methods is being able to describe the wavefunctions at stretched geometries, and hence a complete picture of the PES including the dissociation limit can be computed effectively. Nevertheless, as described above, the success of this example is not guarantee that the approach will work in general for more complicated systems.

$^2B_1$ Feshbach Resonance in H_2O^-

Now that the effectiveness of the projected CAP-MRCI approach has been demonstrated for the calculation of a shape resonance, we turn our attention to computing 2p-1h resonances with the same approach. Since we are employing a multi-reference approach, computing 2p-1h resonances is quite straightforward and effective. This is described in our earlier work where we employ multi-reference approaches with stabilization methods to compute 2p-1h resonances in water and benzene anions.[75] Here, we attempt to describe the lowest Feshbach resonance ($^2B_1$) in H_2O anion. The $^2B_1$ Feshbach resonance has been the subject of several studies over the past years. Experiments by Schulz, Compton et al. and Belić et al. place the resonance position at 6.5 eV with no information on the corresponding width.[96–98] A complete description of the complex potential energy surfaces of the various Feshbach resonances in water has been provided by Haxton et al. using complex Kohn scattering calculations, where they estimate the $^2B_1$ resonance position and width to be 6.09 eV and 10 meV, respectively.[99] On the other hand, R-matrix studies by Gorfinikiel et al. report a position of 6.99 eV and a width of 4 meV.[100] From our previous work

using stabilization-MRCISD, the position and width for the $^2B_1$ resonance is predicted to be 7.2 eV and 7 meV, respectively.[75]

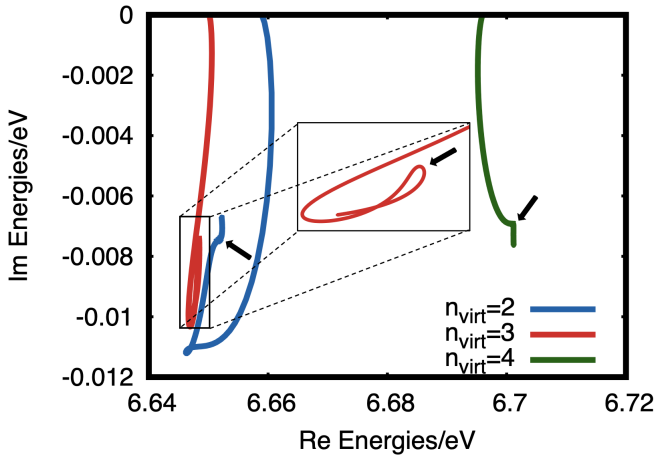

Figure 7: Corrected trajectories for the $^2B_1$ Feshbach resonance in H_2O^- computed at MRCIS(7,5+n_{virt})/aug-cc-pVTZ+[3s3p3d(O)] level of theory. 'n_{virt}' is the number of lowest energy virtual orbitals in the active space for anion calculations. Arrows indicate the turning points.

Table 6: Corrected trajectories for the $^2B_1$ Feshbach resonance in H_2O^- at MRCIS(7,5+n_{virt})/aug-cc-pVTZ+[3s3p3d(O)] level of theory. Box size is fixed at $r_x^0 = 2.72, r_y^0 = 2.40, r_z^0 = 2.60$ a.u..

n_{virt}	U_R (eV)	Γ(eV)	η_{opt}^U (a.u.)
2	6.65	0.015	0.011
3	6.65	0.015	0.0054
4	6.70	0.014	0.0031

Table 6 contains a summary of the computed resonance positions and widths for the $^2B_1$ Feshbach resonance as a function of active space size, whereas the corresponding trajectories are shown in Figure 7. The number of lowest energy virtual orbitals in the active space is increased from 2 to 4 to track the associated changes in the final positions and widths. Unfortunately, the minimum logarithmic velocity criterion was not fulfilled for the uncorrected trajectory and therefore uncorrected results are not presented. The corrected positions remain consistent against changes in the active space at 6.65 eV. A small increase of 0.05 eV is observed in the corrected position for the (7,9) active space. The widths, on the other hand seem to decrease as we add more virtual orbitals into the active space. Our results for the position are in very good agreement with theoretical

and experimental estimates. Also, the theoretical predictions of the width of ≈14 meV is in good agreement with the result of Haxton et al.[99] The widths are also not very sensitive to the active space despite their small value. Since there is no experimental information regarding the widths, a direct comparison of our computed value to experiment is not possible.

Shape and Feshbach Resonances in Maleonitrile and Fumaronitrile Anions

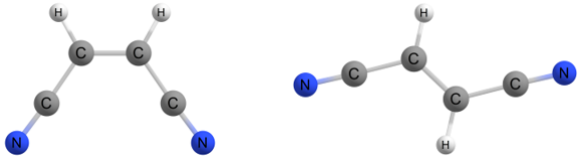

Figure 8: Optimized structures of maleonitrile (MN) (left) and fumaronitrile (FN) (right). The highest Abelian point groups for MN and FN are C_{2v} and C_{2h}, respectively.

A final application of the projected CAP-MRCI method is demonstrated for the computation of both shape and Feshbach resonances in two structural isomers of dicyanoethylene (seen in Fig 8). In this final application we want to examine the effect of mixing between shape and Feshbach resonances on their properties. Very little is known about the resonances in dicyanoethylene anions. Photo-detachment experiments by Khuseynov et al.[101] on the fumaronitrile radical anion (FN) reveal a series of shape resonances in the photo-electron spectrum. The shape resonances correspond to e^- attachment to low-lying valence unoccupied orbitals of fumaronitrile radical anion. The shape resonances have also been detected using electron transmission spectroscopy.[102] There is some theoretical work as well using projected CAP/SAC-CI by Ehara et al.[103] Although there is no experimental observation of the Feshbach resonance in either isomer of dicyanoethylene, which is formed from the e^- attachment to HOMO->LUMO excitation, this has been explored theoretically.[62] A theoretical study by Klaiman and Cederbaum demonstrated that barrierless isomerization reaction can be achieved in either direction by simply accessing the Feshbach resonances in either of the isomers of dicyanoethylene.[62] They were able to compute the potential energy surfaces along the isomerization pathway starting from the Feshbach resonance in either direction by simply performing small basis set calculations. The Feshbach resonances for both isomers radical

anions were predicted to be around $\sim$ 90 kcal mol^{-1} or 3.9 eV.

$^2B_1$ resonances in cis-dicyanoethylene anion

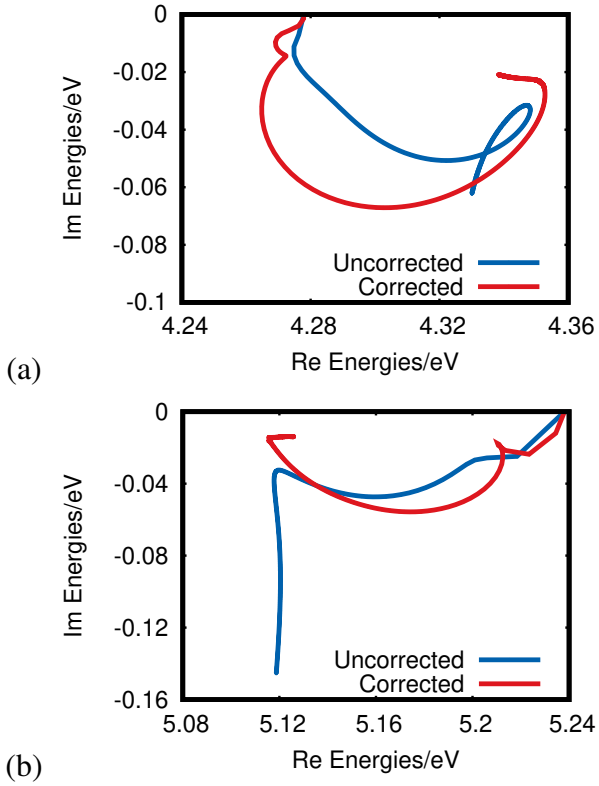

Figure 9: Uncorrected and corrected trajectories for the $^2B_1$ Feshbach (a) and shape (b) resonances in MN anion at MRCIS(7,9)/aug-cc-pVTZ+[3p] level of theory.

In order to obtain both positions and widths we use the projected CAP-MRCI approach to study both one particle and 2p-1h resonances of maleonitrile (MN) anion and the mixing between them. As discussed earlier, the 2p-1h resonance in this case is a Feshbach resonance. The results obtained at the SA12-CAP-MRCIS(7,9)/aug-cc-pVTZ+[3p] level of theory for both the Feshbach and shape resonances of $^2B_1$ symmetry are summarized in Table 7, while details for various box sizes are shown in SI. The uncorrected and corrected trajectories for the Feshbach resonance are depicted in Figure 9. The position is at 4.35 eV, while the width is about 0.05 eV. On the other hand, the shape resonance is situated slightly above the Feshbach with a position of 5.12 eV from the neutral. The energy difference between the shape and the Feshbach resonance is calculated to be 0.77 eV. The

Table 7: Corrected resonance positions and widths of Feshbach and shape resonances in MN and FN anions respectively at SA12-MRCIS(7,9)/aug-cc-pVTZ+[3p] level of theory. The characterization as Feshbach and Shape resonances is based on initial expectations and it is not appropriate for MN, as discussed in the text.

Res. Type	E_R (eV)	Γ(eV)
Feshbach (MN)	4.35	4.7×10^{-2}
Shape (MN)	5.12	3.0×10^{-2}
Feshbach (FN)	4.37	6.8×10^{-3}
Shape (FN)	5.16	3.8×10^{-1}

close proximity of the shape to the Feshbach should result in mixing and this feature is reflected in the CI coefficients associated with the Feshbach resonance wavefunction. The coefficient of the Feshbach configuration is found to be 0.61 and the coefficient corresponding to the shape configuration is observed to be 0.45, indicating strong mixing between the two resonances. To further investigate the mixing, we also looked at the natural orbital occupation numbers for both shape and Feshbach resonance states (Fig 10). The effect of mixing becomes evident when we look at the individual orbital occupation numbers of $2b_1$, $2a_2$ and $3b_1$ orbitals in both shape and Feshbach resonances. The $2b_1$ orbital should be singly occupied for the shape resonance and doubly occupied for the Feshbach resonance. However the occupation numbers are almost equal for the two resonances, around 1.5-1.7. The mixing becomes more evident in the case of the $2a_2$ orbital where the occupation number is only 1 and not > 1.5 to indicate the presence of 2 electrons in the Feshbach resonance. The $2a_2$ orbital in the shape resonance has an occupation number of 0.6 as opposed to being ~ 0.0, indicating the presence of an electron. Similarly, the unoccupied $3b_1$ orbital in the Feshbach resonance has an occupation number of 0.5, although in a single configuration description it should be 0. More importantly the mixing has important consequences for the widths, which are very similar for the two resonances, even though one would expect the Feshbach resonance to be much longer lived. The strong mixing between the two configurations indicates that the characterization of either state as “shape" or “Feshbach" is not appropriate any more. For a clear distinction between the decay channels, computation of partial decay widths is required. As we will discuss, the same effect in trans-dicyanoethylene presents an

alternate picture altogether.

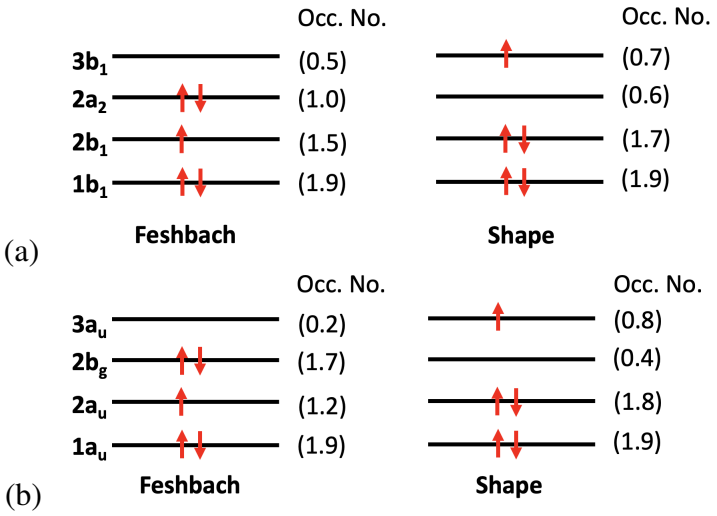

Figure 10: Natural orbital occupation numbers for the Feshbach and shape resonances of MN (a) and FN (b) using MRCIS(7,9)/aug-cc-pVTZ+[3p].

^2A_u resonances in trans-dicyanoethylene

The energy positions and widths of the Feshbach and shape resonances for FN are tabulated in Table 7. The trajectory for the Feshbach resonance is shown in Figure 11. Since the minimum of the logarithmic velocity couldn't be identified for the uncorrected trajectory, the results are therefore omitted from the figure. Detailed results are shown in the SI. From the corrected results for the ^2A_u Feshbach resonance, the position is situated at an energy of 4.37 eV from the neutral FN. The position of the Feshbach in FN anion is similar to the 4.35 eV position seen in the case of the MN anion. The widths, however are different by an order of magnitude between the two resonances. In the case of the MN anion, the width was reported to be 0.047 eV but for the Feshbach in FN anion, it is predicted to be an order of magnitude smaller, 0.0068 eV. This much smaller width is more in line with what would be expected from a Feshbach resonance. A shape resonance is also seen here of ^2A_u symmetry situated at an energy of 5.16 eV. The width for the shape resonance as seen from Table 7 is 0.38 eV, indicating a broad π^* resonance as opposed to the shape resonance in MN anion. Experimental results by Burrow et al.[102] place the ^2A_u resonance

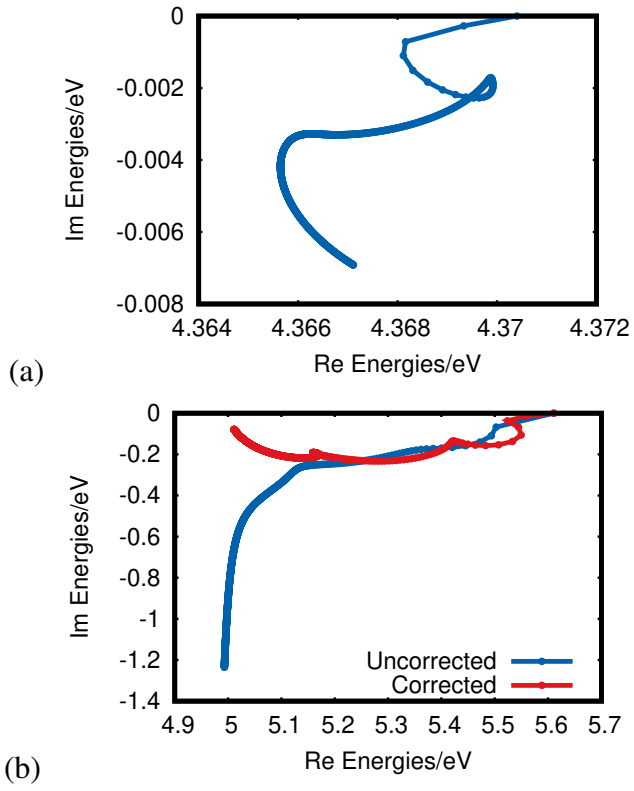

Figure 11: (a) Corrected trajectory for the ^2A_u Feshbach resonance. (b) Uncorrected and corrected trajectories for the ^2A_u shape resonance in FN anion. MRCIS(7,9)/aug-cc-pVTZ+[3p] level of theory was used in both cases.

position at 3.5 eV. Projected CAP/SAC-CI results by Ehara et al.[103] report a position of 4.21 eV and a width of 0.36 eV for the same resonance. Our results for the width are in good agreement, but our position is off by 1.66 eV from the experimental value.

The extent of mixing between the Feshbach and shape resonances in FN^- is very different from MN^-. In the case of the FN anion, the wavefunction of the Feshbach resonance has a CI coefficient of 0.81 from the Feshbach configuration but only a coefficient of 0.32 from the shape configuration. The relatively lower mixing in the trans-isomer is also evident from the analysis of natural orbital occupation numbers shown in Figure 10b, which in this case are aligned with the expected occupations for Feshbach and shape resonances.

Comparison of these two isomers provides evidence of the profound effect of mixing. When mixing occurs the widths of the two channels are very similar, as seen in MN, while without mixing they differ by two orders of magnitude, as seen in FN. In order to confirm that the mixing

is responsible for the different widths, we calculated the shape resonances of the two isomers using EOM-EA-CCSD where mixing with Feshbach resonances is not possible. The detailed results are shown in SI. Remarkably, we found that both isomers have similar large widths, around 0.3-0.5 eV. So the small width and associated long lifetime for the shape resonance in MN is clearly an effect of mixing with the Feshbach resonance. This finding can be very important in a variety of molecules where mixing has been suggested, and in particular the nucleobases.[71] This is the first time that accurate widths have been calculated confirming the importance of mixing.

Conclusions

An implementation of the projected CAP approach with the MRCI electronic structure method is presented. The freely available OpenCAP program is interfaced to the open-source COLUMBUS electronic structure program system to compute η-trajectories for resonances at the cost of a single MRCI calculation. The projected approach is employed to study shape and Feshbach resonances in anions of N_2, H_2O and isomers of dicyanoethylene.

Benchmark studies on the $^2\Pi_g$ resonance in the N_2 anion with projected CAP-MRCI suggest that a small subspace consisting of a few states is adequate for the characterization of resonance states to a reasonable accuracy. We also demonstrated the variation of resonance positions and widths against the changes in convergence thresholds for pseudo-continuum states, where we observed that the final resonance energies remain relatively insensitive to changes in the convergence criterion for pseudo-continuum states. This observation is in contrast to stabilization methods, where the eigenvalues in the vicinity of the resonance state need to be converged tightly for the successful application of the analytical continuation procedure to retrieve Siegert energies.

Moving from single point energies, we know that MRCI excels in producing complete potential energy surfaces for bound states and in this work, we were able to generate a smooth complex potential energy surface for an anion resonance using the projected CAP-MRCI approach. The advantage of the projected CAP-MRCI for the computation of complex potential energy surfaces is

twofold: 1) projected CAP is computationally inexpensive compared to conventional CAP implementation for the computation of single point energies; 2) use of MRCI as the underlying electronic structure method enables us to explore regions of the potential energy surfaces where multiple configurations are dominant. Another advantages of MRCI when studying potential energy surfaces is that it can be applied to conical intersections. Consequently, it will be interesting to investigate the applicability of the CAP-MRCI approach to compute resonance energies for molecular geometries in the vicinity of complex analogues of conical intersections. As demonstrated by Feuerbacher et al.[46] and Benda et al.,[58] crossings between resonances are quite common, and their characterization is important for a deeper understanding of the underlying decay mechanisms. Although the current work successfully reproduced the PES of N_2^- more work is needed to examine the behavior of complex PES for more complicated molecules.

To demonstrate the effectiveness of the projected CAP-MRCI approach, both Feshbach and shape resonances in structural isomers of dicyanoethylene and the mixing between the two resonances in respective isomers were investigated. We found that in both isomers, the positions of the Feshbach and shape resonances are similar. However, a key difference between the isomers is that in the case of the cis-isomer, the resonant-channel mixing is greater compared to that of the trans-isomer. As a consequence we observe very different widths and lifetimes between the two isomers. The cis-isomer has a much longer lifetime of the shape resonance in comparison to the shape resonance in trans-isomer. Since mixing between different types of resonances is present in many systems, including the biologically relevant nucleobases, we expect this observed effect on the widths to have profound effects in electron driven processes.

Despite the above described advantages of CAP-MRCI, there are also some shortcomings of using multi-reference methods as the underlying electronic structure method in CAP based calculations. A main issue is that, since the resonance position is computed by taking the difference between the neutral and anion energies obtained from two different calculations, the final values are usually over-estimated. In addition, the dependence of resonance parameters on choice of active space also needs to be included while dealing with multi-reference methods unlike single-reference

methods.

Acknowledgement

We acknowledge support by the National Science Foundation (NSF, grant number: CHE-1800171). This work used the Extreme Science and Engineering Discovery Environment (XSEDE), which is supported by National Science Foundation grant number ACI-1548562.

Supporting Information Available

The supplementary information consists of the cartesian coordinates, active spaces of molecules used in the study, and additional results for N_2, MN and FN resonances.

References

(1) Mason, N. J.; Nair, B.; Jheeta, S.; Szymańska, E. Electron induced chemistry: a new frontier in astrochemistry. *Faraday Discuss.* **2014**, *168*, 235–247.

(2) Boyer, M. C.; Rivas, N.; Tran, A. A.; Verish, C. A.; Arumainayagam, C. R. The role of low-energy ($\leq$ 20 eV) electrons in astrochemistry. *Surf. Sci.* **2016**, *652*, 26–32.

(3) Bass, A. D.; Sanche, L. Dissociative electron attachment and charge transfer in condensed matter. *Radiat. Phys. Chem.* **2003**, *68*, 3–13.

(4) Arumainayagam, C. R.; Lee, H.-L.; Nelson, R. B.; Haines, D. R.; Gunawardane, R. P. Low-energy electron-induced reactions in condensed matter. *Surf. Sci. Rep.* **2010**, *65*, 1–44.

(5) Boudaiffa, B.; Cloutier, P.; Hunting, D.; Huels, M. A.; Sanche, L. Resonant formation of DNA strand breaks by low-energy (3 to 20 eV) electrons. *Science* **2000**, *287*, 1658–1660.

(6) Tonzani, S.; Greene, C. H. Low-energy electron scattering from DNA and RNA bases: Shape resonances and radiation damage. *J. Chem. Phys.* **2006**, *124*, 054312.

(7) Li, Z.; Cloutier, P.; Sanche, L.; Wagner, J. R. Low-energy electron-induced DNA damage: Effect of base sequence in oligonucleotide trimers. *J. Am. Chem. Soc.* **2010**, *132*, 5422–5427.

(8) Ren, X.; Jabbour Al Maalouf, E.; Dorn, A.; Denifl, S. Direct evidence of two interatomic relaxation mechanisms in argon dimers ionized by electron impact. *Nat. Commun.* **2016**, *7*, 1–6.

(9) Wang, E.; Ren, X.; Baek, W.; Rabus, H.; Pfeifer, T.; Dorn, A. Water acting as a catalyst for electron-driven molecular break-up of tetrahydrofuran. *Nat. Commun.* **2020**, *11*, 1–7.

(10) Ren, X.; Wang, E.; Skitnevskaya, A. D.; Trofimov, A. B.; Gokhberg, K.; Dorn, A. Experimental evidence for ultrafast intermolecular relaxation processes in hydrated biomolecules. *Nat. Phys.* **2018**, *14*, 1062–1066.

(11) Ren, X.; Zhou, J.; Wang, E.; Yang, T.; Xu, Z.; Sisourat, N.; Pfeifer, T.; Dorn, A. Ultrafast energy transfer between π-stacked aromatic rings upon inner-valence ionization. *Nat. Chem.* **2022**, *14*, 232–238.

(12) Combes, J.-M.; Duclos, P.; Klein, M.; Seiler, R. The shape resonance. *Commun. Math. Phys.* **1987**, *110*, 215–236.

(13) Moiseyev, N. *Non-Hermitian quantum mechanics*; Cambridge University Press, 2011.

(14) Herbert, J. M. The quantum chemistry of loosely bound electrons. *Rev. Comput. Chem.* **2015**, *28*, 391–517.

(15) Domcke, W. Theory of resonance and threshold effects in electron-molecule collisions: The projection-operator approach. *Phys. Rep.* **1991**, *208*, 97–188.

(16) Moiseyev, N. Quantum theory of resonances: calculating energies, widths and cross-sections by complex scaling. *Phys. Rep.* **1998**, *302*, 212–293.

(17) Tennyson, J. Electron–molecule collision calculations using the R-matrix method. *Phys. Rep.* **2010**, *491*, 29–76.

(18) Simons, J. Theoretical study of negative molecular ions. *Annu. Rev. Phys. Chem.* **2011**, *62*, 107–128.

(19) da Costa, R. F.; Varella, M. T. d. N.; Bettega, M. H.; Lima, M. A. Recent advances in the application of the Schwinger multichannel method with pseudopotentials to electron-molecule collisions. *Eur. Phys. J. D* **2015**, *69*, 1–24.

(20) Jagau, T.-C.; Bravaya, K. B.; Krylov, A. I. Extending quantum chemistry of bound states to electronic resonances. *Annu. Rev. Phys. Chem.* **2017**, *68*, 525–553.

(21) Rescigno, T. N.; Lengsfield, B. H. I.; McCurdy, C. W. In *Modern Electronic Structure Theory: Part I in Advanced Series in Physical Chemistry*; Yarkony, D. R., Ed.; World Scientific Publishing Company: Singapore, 1995; p 501.

(22) Rescigno, T., McKoy, V., Schneider, B., Eds. *Electron-Molecule and Photon-Molecule Collisions*; Plenum, New York, 1979.

(23) Burke, P., Berrington, K., Eds. *Atomic and Molecular Processes: An R-Matrix Approach*; IOP Publishing, Bristol., 1993.

(24) Winstead, C.; McKoy, V. Electron Scattering by Small Molecules. *Adv. Chem. Phys.* **1996**, *96*, 103.

(25) Bartschat, K.; Burke, P. The R-matrix method for electron impact ionisation. *J. Phys. B: At. Mol. Phys.* **1987**, *20*, 3191.

(26) Lima, M. A.; Brescansin, L. M.; da Silva, A. J.; Winstead, C.; McKoy, V. Applications of the Schwinger multichannel method to electron-molecule collisions. *Phys. Rev. A* **1990**, *41*, 327.

(27) Santra, R.; Cederbaum, L. S. Non-Hermitian electronic theory and applications to clusters. *Phys. Rep.* **2002**, *368*, 1–117.

(28) Morgan, J.; Simon, B. The calculation of molecular resonances by complex scaling. *J. Phys. B: At. Mol. Phys.* **1981**, *14*, L167.

(29) Reinhardt, W. P. Complex Coordinates in the Theory of Atomic and Molecular Structure and Dynamics. *Annu. Rev. Phys. Chem.* **1982**, *33*, 223–255.

(30) McCurdy Jr, C.; Rescigno, T. Extension of the method of complex basis functions to molecular resonances. *Phys. Rev. Lett.* **1978**, *41*, 1364.

(31) White, A. F.; Head-Gordon, M.; McCurdy, C. W. Complex basis functions revisited: Implementation with applications to carbon tetrafluoride and aromatic N-containing heterocycles within the static-exchange approximation. *J. Chem. Phys.* **2015**, *142*, 054103.

(32) White, A. F.; Epifanovsky, E.; McCurdy, C. W.; Head-Gordon, M. Second order Møller-Plesset and coupled cluster singles and doubles methods with complex basis functions for resonances in electron-molecule scattering. *J. Chem. Phys.* **2017**, *146*, 234107.

(33) Riss, U.; Meyer, H.-D. Calculation of resonance energies and widths using the complex absorbing potential method. *J. Phys. B: At. Mol. Opt.* **1993**, *26*, 4503.

(34) Sommerfeld, T.; Riss, U.; Meyer, H.; Cederbaum, L.; Engels, B.; Suter, H. Temporary anions-calculation of energy and lifetime by absorbing potentials: The resonance. *J. Phys. B: At. Mol. Opt. Phys.* **1998**, *31*, 4107.

(35) Ben-Asher, A.; Moiseyev, N. On the equivalence of different methods for calculating resonances: From complex Gaussian basis set to reflection-free complex absorbing potentials

via the smooth exterior scaling transformation. *J. Chem. Theory Comput.* **2016**, *12*, 2542–2552.

(36) Siegert, A. J. On the derivation of the dispersion formula for nuclear reactions. *Phys. Rev.* **1939**, *56*, 750.

(37) Jordan, K. D.; Voora, V. K.; Simons, J. *Thom H. Dunning, Jr.*; Springer, 2015; pp 85–99.

(38) Sajeev, Y.; Santra, R.; Pal, S. Analytically continued Fock space multireference coupled-cluster theory: Application to the $^2\Pi_g$ shape resonance in $e - N_2$ scattering. *J. Chem. Phys.* **2005**, *122*, 234320.

(39) Ghosh, A.; Vaval, N.; Pal, S. Equation-of-motion coupled-cluster method for the study of shape resonance. *J. Chem. Phys.* **2012**, *136*, 234110.

(40) Sajeev, Y.; Ghosh, A.; Vaval, N.; Pal, S. Coupled cluster methods for autoionisation resonances. *Int. Rev. Phys. Chem.* **2014**, *33*, 397–425.

(41) Basumallick, S.; Sajeev, Y.; Pal, S.; Vaval, N. Negative ion resonance states: The Fock-space coupled-cluster way. *J. Phys. Chem. A* **2020**, *124*, 10407–10421.

(42) Zuev, D.; Jagau, T.-C.; Bravaya, K. B.; Epifanovsky, E.; Shao, Y.; Sundstrom, E.; Head-Gordon, M.; Krylov, A. I. Complex absorbing potentials within EOM-CC family of methods: Theory, implementation, and benchmarks. *J. Chem. Phys.* **2014**, *141*, 024102.

(43) Sajeev, Y.; Pal, S. A general formalism of the Fock space multireference coupled cluster method for investigating molecular electronic resonances. *Mol. Phys.* **2005**, *103*, 2267–2275.

(44) Dempwolff, A. L.; Belogolova, A. M.; Sommerfeld, T.; Trofimov, A. B.; Dreuw, A. CAP/EA-ADC method for metastable anions: Computational aspects and application to π^* resonances of norbornadiene and 1, 4-cyclohexadiene. *J. Chem. Phys.* **2021**, *155*, 054103.

(45) Santra, R.; Cederbaum, L. Complex absorbing potentials in the framework of electron propagator theory. I. General formalism. *J. Chem. Phys.* **2002**, *117*, 5511–5521.

(46) Feuerbacher, S.; Sommerfeld, T.; Santra, R.; Cederbaum, L. Complex absorbing potentials in the framework of electron propagator theory. II. Application to temporary anions. *J. Chem. Phys.* **2003**, *118*, 6188–6199.

(47) Kanazawa, Y.; Ehara, M.; Sommerfeld, T. Low-Lying π^* Resonances of Standard and Rare DNA and RNA Bases Studied by the Projected CAP/SAC–CI Method. *J. Phys. Chem. A* **2016**, *120*, 1545–1553.

(48) Sommerfeld, T. Resonance States of Atomic Di-anions. *Phys. Rev. Lett.* **2000**, *85*, 956.

(49) Sommerfeld, T.; Santra, R. Efficient method to perform CAP/CI calculations for temporary anions. *Int. J. Quantum Chem.* **2001**, *82*, 218–226.

(50) Kunitsa, A. A.; Granovsky, A. A.; Bravaya, K. B. CAP-XMCQDPT2 method for molecular electronic resonances. *J. Chem. Phys.* **2017**, *146*, 184107.

(51) Phung, Q. M.; Komori, Y.; Yanai, T.; Sommerfeld, T.; Ehara, M. Combination of a Voronoi-type complex absorbing potential with the XMS-CASPT2 method and pilot applications. *J. Chem. Theory Comput.* **2020**, *16*, 2606–2616.

(52) Das, S.; Sajeev, Y.; Samanta, K. An Electron Propagator Approach Based on a Multiconfigurational Reference State for the Investigation of Negative-Ion Resonances Using a Complex Absorbing Potential Method. *J. Chem. Theory Comput.* **2020**, *16*, 5024–5034.

(53) Zhou, Y.; Ernzerhof, M. Open-System Kohn-Sham Density Functional Theory. *J. Chem. Phys.* **2012**, *136*, 094105.

(54) Zhou, Y.; Ernzerhof, M. Calculating the Lifetimes of Metastable States with Complex Density Functional Theory. *J. Phys. Chem. Lett.* **2012**, *3*, 1916–1920.

(55) Gayvert, J. R.; Bravaya, K. B. Projected CAP-EOM-CCSD method for electronic resonances. *J. Chem. Phys.* **2022**, *156*, 094108.

(56) Benda, Z.; Jagau, T.-C. Communication: Analytic gradients for the complex absorbing potential equation-of-motion coupled-cluster method. *J. Chem. Phys.* **2017**, *146*, 031101.

(57) Benda, Z.; Jagau, T.-C. Understanding processes following resonant electron attachment: Minimum-energy crossing points between anionic and neutral potential energy surfaces. *J. Chem. Theory. Comput.* **2018**, *14*, 4216–4223.

(58) Benda, Z.; Jagau, T.-C. Locating exceptional points on multidimensional complex-valued potential energy surfaces. *J. Phys. Chem. Lett.* **2018**, *9*, 6978–6984.

(59) Al-Saadon, R.; Shiozaki, T.; Knizia, G. Visualizing Complex-Valued Molecular Orbitals. *J. Phys. Chem. A* **2019**, *123*, 3223–3228.

(60) Thodika, M.; Fennimore, M.; Karsili, T. N.; Matsika, S. Comparative study of methodologies for calculating metastable states of small to medium-sized molecules. *J. Chem. Phys.* **2019**, *151*, 244104.

(61) Santra, R.; Cederbaum, L. S. An efficient combination of computational techniques for investigating electronic resonance states in molecules. *J. Chem. Phys.* **2001**, *115*, 6853–6861.

(62) Klaiman, S.; Cederbaum, L. S. Barrierless Single-Electron-Induced cis–trans Isomerization. *Angew. Chem.* **2015**, *127*, 10616–10619.

(63) Davis, D.; Vysotskiy, V. P.; Sajeev, Y.; Cederbaum, L. S. Electron Impact Catalytic Dissociation: Two-Bond Breaking by a Low-Energy Catalytic Electron. *Angew. Chem. Int. Ed.* **2011**, *50*, 4119–4122.

(64) Davis, D.; Vysotskiy, V.; Sajeev, Y.; Cederbaum, L. A One-Step Four-Bond-Breaking Reaction Catalyzed by an Electron. *Angew. Chem. Int. Ed.* **2012**, *51*, 8003–8007.

(65) Davis, D.; Bhushan, K.; Sajeev, Y.; Cederbaum, L. A Concerted Synchronous [2+ 2] Cycloreversion Repair Catalyzed by Two Electrons. *J. Chem. Phys. Lett.* **2018**, *9*, 6973–6977.

(66) Davis, D.; Kundu, S.; Prabhudesai, V.; Sajeev, Y.; Krishnakumar, E. Formation of CO2 from formic acid through catalytic electron channel. *J. Chem. Phys.* **2018**, *149*, 064308.

(67) Kawarai, Y.; Weber, T.; Azuma, Y.; Winstead, C.; McKoy, V.; Belkacem, A.; Slaughter, D. Dynamics of the dissociating uracil anion following resonant electron attachment. *J. Chem. Phys. Lett.* **2014**, *5*, 3854–3858.

(68) Bochenkova, A. V.; Klærke, B.; Rahbek, D. B.; Rajput, J.; Toker, Y.; Andersen, L. H. UV Excited-State Photoresponse of Biochromophore Negative Ions. *Angew. Chem. Int. Ed.* **2014**, *53*, 9797–9801.

(69) Fennimore, M. A.; Karsili, T. N.; Matsika, S. Mechanisms of H and CO loss from the uracil nucleobase following low energy electron irradiation. *Phys. Chem. Chem. Phys.* **2017**, *19*, 17233–17241.

(70) Alizadeh, E.; Orlando, T. M.; Sanche, L. Biomolecular damage induced by ionizing radiation: the direct and indirect effects of low-energy electrons on DNA. *Annu. Rev. Phys. Chem.* **2015**, *66*, 379–398.

(71) Fennimore, M. A.; Matsika, S. Electronic resonances of nucleobases using stabilization methods. *J. Phys. Chem. A* **2018**, *122*, 4048–4057.

(72) Loupas, A.; Gorfinkiel, J. D. Shape and core-excited resonances in electron scattering from alanine. *J. Chem. Phys.* **2019**, *150*, 064307.

(73) Regeta, K.; Allan, M.; Masín, Z.; Gorfinkiel, J. Absolute cross sections for electronic excitation of pyrimidine by electron impact. *J. Chem. Phys. 144*, 024302.

(74) Winstead, C.; McKoy, V. Resonant channel coupling in electron scattering by pyrazine. *Phys. Rev. Lett.* **2007**, *98*, 113201.

(75) Thodika, M.; Mackouse, N.; Matsika, S. Description of Two-Particle One-Hole Electronic Resonances Using Orbital Stabilization Methods. *J. Phys. Chem. A* **2020**, *124*, 9011–9020.

(76) Masin, Z.; Gorfinkiel, J. D. Shape and core excited resonances in electron collisions with diazines. *J Chem Phys* **2012**, *137*, 204312.

(77) Lischka, H.; Shepard, R.; Shavitt, I.; Pitzer, R.; Dallos, M.; Müller, T.; Szalay, P.; Brown, F.; Ahlrichs, R.; Boehm, H. COLUMBUS, an ab initio electronic structure program, release 7.0. *COLUMBUS, an ab initio electronic structure program, release 7.0* **2017**,

(78) Lischka, H.; Shepard, R.; Müller, T.; Szalay, P. G.; Pitzer, R. M.; Aquino, A. J.; Araújo do Nascimento, M. M.; Barbatti, M.; Belcher, L. T.; Blaudeau, J.-P. The generality of the GUGA MRCI approach in COLUMBUS for treating complex quantum chemistry. *J. Chem. Phys.* **2020**, *152*, 134110.

(79) Gayvert, J. OpenCAP. `https://github.com/gayverjr/opencap`, 2021.

(80) Santra, R.; Cederbaum, L.; Meyer, H.-D. Electronic decay of molecular clusters: non-stationary states computed by standard quantum chemistry methods. *Chem. Phys. Lett.* **1999**, *303*, 413–419.

(81) Ehara, M.; Sommerfeld, T. CAP/SAC-CI method for calculating resonance states of metastable anions. *Chem. Phys. Lett.* **2012**, *537*, 107–112.

(82) Maier, C.; Cederbaum, L.; Domcke, W. A spherical-box approach to resonances. *J. Phys. B: At. Mol. Phys.* **1980**, *13*, L119.

(83) Sommerfeld, T.; Ehara, M. Complex absorbing potentials with Voronoi isosurfaces wrapping perfectly around molecules. *J. Chem Theory Comput.* **2015**, *11*, 4627–4633.

(84) Gayvert, J.; Bravaya, K. CAP-EOM-CCSD method with smooth Voronoi CAP for metastable electronic states in molecular clusters. *ChemRxiv* **2020**,

(85) Jagau, T.-C.; Zuev, D.; Bravaya, K. B.; Epifanovsky, E.; Krylov, A. I. A Fresh Look at Resonances and Complex Absorbing Potentials: Density Matrix-Based Approach. *J. Phys. Chem. Lett.* **2014**, *5*, 310.

(86) Lischka, H.; Shepard, R.; Pitzer, R. M.; Shavitt, I.; Dallos, M.; Müller, T.; Szalay, P. G.; Seth, M.; Kedziora, G. S.; Yabushita, S. High-level multireference methods in the quantum-chemistry program system COLUMBUS: Analytic MR-CISD and MR-AQCC gradients and MR-AQCC-LRT for excited states, GUGA spin–orbit CI and parallel CI density. *Phys. Chem. Chem. Phys.* **2001**, *3*, 664–673.

(87) Lischka, H.; Müller, T.; Szalay, P. G.; Shavitt, I.; Pitzer, R. M.; Shepard, R. Columbus–a program system for advanced multireference theory calculations. *WIREs: Comp. Mol. Sci.* **2011**, *1*, 191–199.

(88) Berman, M.; Estrada, H.; Cederbaum, L. S.; Domcke, W. Nuclear dynamics in resonant electron-molecule scattering beyond the local approximation: The 2.3-eV shape resonance in N_2. *Phys. Rev. A* **1983**, *28*, 1363.

(89) Hazi, A. U.; Rescigno, T. N.; Kurilla, M. Cross sections for resonant vibrational excitation of N_2 by electron impact. *Phys. Rev. A* **1981**, *23*, 1089.

(90) Meyer, H.-D. Optical potentials for electron-molecule scattering: A comparative study on the N_2 $^2\Pi_g$ resonance. *Phys. Rev. A* **1989**, *40*, 5605.

(91) Davidson, E. R. The iterative calculation of a few of the lowest eigenvalues and corresponding eigenvectors of large real-symmetric matrices. *J. Comput. Phys.* **1975**, *17*, 87–94.

(92) Liu, B. The simultaneous expansion method for the iterative solution of several of the lowest-lying eigenvalues and corresponding eigenvectors of large real-symmetric matrices. *Numerical Algorithms in Chemistry: Algebraic Methods* **1978**, 49–53.

(93) Non-iterative triple excitations in equation- of-motion coupled-cluster theory for electron attachment with applications to bound and temporary anions. *J. Chem. Phys.* **2018**, *148*, 024104.

(94) Sajeev, Y.; Vysotskiy, V.; Cederbaum, L.; Moiseyev, N. Continuum remover-complex absorbing potential: Efficient removal of the nonphysical stabilization points. *J. Chem. Phys.* **2009**, *131*, 211102.

(95) Jagau, T.-C.; Krylov, A. I. Complex absorbing potential equation-of-motion coupled-cluster method yields smooth and internally consistent potential energy surfaces and lifetimes for molecular resonances. *J. Phys. Chem. Lett.* **2014**, *5*, 3078–3085.

(96) Schulz, G. Excitation and negative ions in H_2O. *J. Chem. Phys.* **1960**, *33*, 1661–1665.

(97) Compton, R.; Christophorou, L. Negative-ion formation in H_2O and D_2O. *Phys. Rev.* **1967**, *154*, 110.

(98) Belic, D.; Landau, M.; Hall, R. Energy and angular dependence of $H^-(D^-)$ ions produced by dissociative electron attachment to H_2O (D_2O). *J. Phys. B: At. Mol. Phys.* **1981**, *14*, 175.

(99) Haxton, D. J.; McCurdy, C. W.; Rescigno, T. N. Dissociative electron attachment to the H_2O molecule I. Complex-valued potential-energy surfaces for the $^2B_1$, $^2A_1$, and $^2B_2$ metastable states of the water anion. *Phys. Rev. A* **2007**, *75*, 012710.

(100) Gorfinkiel, J.; Morgan, L.; Tennyson, J. Electron impact dissociative excitation of water within the adiabatic nuclei approximation. *J. Phys. B: At. Mol. Phys.* **2002**, *35*, 543.

(101) Khuseynov, D.; Dixon, A. R.; Dokuchitz, D. J.; Sanov, A. Photochemistry of fumaronitrile radical anion and its clusters. *J. Phys. Chem. A* **2014**, *118*, 4510–4518.

(102) Burrow, P.; Howard, A.; Johnston, A.; Jordan, K. Temporary anion states of hydrogen cyanide, methyl cyanide, and methylene dicyanide, selected cyanoethylenes, benzonitrile, and tetracyanoquinodimethane. *J. Phys. Chem.* **1992**, *96*, 7570–7578.

(103) Ehara, M.; Kanazawa, Y.; Sommerfeld, T. Low-lying π^* resonances associated with cyano groups: A CAP/SAC-CI study. *Chem. Phys.* **2017**, *482*, 169–177.

TOC Graphic